IEEE Robotics and Automation Letters (RA-L) paper, presented at ICRA 2026, Vienna, Austria. Cite as RA-L paper.

Optimization of Preemptive Impact Mitigation Without Prior Collision Testing

Hayato Nakamura, Hikaru Arita, *Member, IEEE*, Shunsuke Tokiwa, and Kenji Tahara, *Member, IEEE*

***Abstract*—Effective impact mitigation strategies are crucial for preventing potential damage to both robotic systems and their operational environments during high-velocity and dynamic maneuvers, as well as during the execution of high-precision tasks. The successful implementation of impact mitigation strategies in real-world applications fundamentally requires appropriate parameter tuning. However, owing to the destructive nature of collisions, heuristic parameter tuning is impractical, as it risks damage to both the robotic system and its operational environment during experimental trials. This study eliminates the need for preliminary collision experiments in parameter optimization by introducing a novel methodology that leverages recent proximity sensor-based preemptive impact mitigation strategies that reframe impact mitigation as a geometric rather than physical problem. The key innovation of this work lies in the reformulation of the proximity sensor output to enable both the analytical derivation of preemptive motion trajectories and the direct application of standard optimization solvers. The effectiveness of the proposed methodology is validated through numerical simulations and two different experimental configurations. By eliminating the need for collision trials, robotic systems can safely execute potentially destructive tasks that would otherwise result in system damage without proper impact mitigation.**

***Index Terms*—Force control, sensor-based control, optimization and optimal control, optical proximity sensor, impact mitigation.**

I. Introduction

CONTACT is a crucial aspect of robot interaction with the environment [1]. However, impacts may cause damage to robots or their surroundings when robots perform tasks that involve physical contact, such as grasping fragile objects, landing for legged robots [2], [3], or safely control for collaborative robots [4], [5]. Accordingly, numerous impact mitigation strategies have been extensively investigated in previous works, such as the implementation of soft materials [6], variable-stiffness actuators [7], and force control schemes [8].

However, impact mitigation methods generally involve inherent trade-offs: while soft materials provide enhanced impact mitigation capabilities, they adversely affect positional control accuracy. The impact mitigation strategy must be optimally designed according to the specific requirements of the target application. These common impact mitigation approaches rely on physical principles; however, mechanical analysis and dynamic simulation of collisions remain challenging because of their discontinuous and instantaneous nature. Consequently, parameters are typically determined through trial and error during task execution or on the basis of users' experience. However, since collisions are inherently destructive phenomena, trial-and-error parameter adjustment can be impractical or infeasible. The primary purpose of implementing impact mitigation techniques is to prevent damage to both the robotic system and its surrounding environment during task execution; destroying these components during preliminary parameter tuning trials would defeat this fundamental objective.

Another category of impact mitigation methods using proximity sensors has recently emerged [9], [10], [11], [12], [13], [14]. Proximity sensors, noncontact sensing devices, offer several advantages in impact mitigation applications; notably, their compact size allows direct integration into the contact surface, minimizing occlusion problems that commonly occur with external sensors such as cameras. Additionally, their rapid response characteristics enable the generation of reactive motions when approaching objects. Leveraging these sensing capabilities, impact mitigation strategies based on proximity sensing are used to resolve the mitigation problem from a geometric perspective rather than a physical one. Specifically, these strategies generate robot motions that minimize the relative velocity between the contact point and the environment. The effectiveness of relative velocity reduction in impact mitigation is based on diminishing the instantaneous momentum change during the collision process [15], [16]. Among the available proximity-based approaches, Arita et al. proposed a combined approach that integrates preemptive impact mitigation using proximity sensors with force control, which requires no switching control law while avoiding mutual interference among the control parameters of each feature [13]. Specifically, the approach proposed in [13] enables independent parameter design for impact mitigation, separating these parameters from the parameters used in postcontact task execution.

In this study, we propose a novel parameter design methodology for impact mitigation that eliminates the need for preliminary collision trials by leveraging the geometric preemptive approach [13]. First, we model the proximity sensor output using exponential functions. While the motion generated in [13] was represented by a noncontinuous nonlinear differential equation, as described in Section II, we demonstrate that modeling the sensor output with exponential functions reformulates the preemptive motion process via analytically tractable differential equations. The reformulation into an analytically tractable model enables the use of standard optimization solvers

Received 30 March 2025; accepted 4 June 2025. Date of publication 20 June 2025; date of current version 30 June 2025. This article was recommended for publication by Associate Editor Y. Wang and Editor A. Kheddar upon evaluation of the reviewers' comments. This work was supported byJSPS KAKENHI under GrantJP20K14702. *(Hayato Nakamura and Hikaru Arita are co-first authors.) (Corresponding author: Hikaru Arita.)*

The authors are with the Department of Mechanical Engineering, Kyushu University, Fukuoka 819-0395, Japan (e-mail: nakamura@hcr.mech.kyushu-u.ac.jp; arita@ieee.org; tokiwa@hcr.mech.kyushu-u.ac.jp; tahara@ieee.org).

Digital Object Identifier 10.1109/LRA.2025.3582137

IEEE Robotics and Automation Letters (RA-L) paper, presented at ICRA 2026, Vienna, Austria. Cite as RA-L paper.

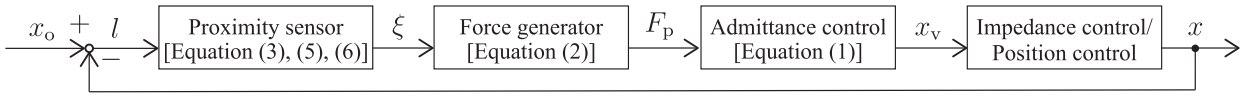

Fig. 1. Block diagram showing an overview of the impact mitigation method. Three sensor output models are investigated for the "proximity sensor" block in this letter.

for parameter design. The details of this reformulation process and optimization approach are presented in Section III.

Although optical reflective proximity sensors, such as those employed in [13], are commonly modeled on the basis of the inverse square law derived from energy diffusion principles [17], [18], [19], exponential-based modeling of sensor output is an alternative approach supported by several previous studies [20], [21]. Oprzędkiewicz and Garbacz [20] proposed a proximity sensor model using the Mittag-Leffler function. The one-parameter Mittag-Leffler function is a generalization of the exponential function. Suzuki et al. [21] showed that a net-structure proximity sensor [22] can fit an exponential function with an exponent expressed as a linear function.

This letter demonstrates that exponential functions with first-order and second-order polynomials in their exponents can be used to achieve our objective. The exponential-based model with a first-order exponent enables representation of the impact mitigation motion as a linear differential equation, which allows us to utilize its analytical solution in the optimization process. Moreover, a model with a second-order exponent provides better fitting accuracy for actual proximity sensor outputs than does an exponential-based model with a first-order exponent. Furthermore, under certain assumptions, the second-order model can also be incorporated into the optimization process.

In summary, this study's contributions are listed as follows:

- This study introduces a novel parameter design methodology for impact mitigation that eliminates the need for preliminary collision trials. Our proposal eliminates the risk of damaging both robotic systems and their environments during trial-and-error parameter adjustment through collision experiments.
- We present two exponential function-based models for proximity sensor outputs and demonstrate their respective advantages. One has advantages in analytical tractability and the other has superior approximation accuracy. These models would facilitate optimization and controller design problems involving proximity sensors beyond the specific objective addressed in this study.

The rest of this letter is organized as follows. In Section II, the problem setting is clarified using equations, and in Section III, proximity sensor models, models of impact mitigation behavior, and parameter design methods are introduced. Section IV presents a comparison of the models, and in Section V, the optimization results and impact mitigation features are presented. In Section VI, the differences between the characteristics of the two models and methods are discussed. Finally, Section VII concludes this study.

II. Problem Statement

In the previous method [13] shown in Fig. 1, the motion of a virtual object is modeled using an approach analogous to admittance control, with the virtual force F_p as the input, as follows:

$$M_\mathrm{a}(\ddot{x}_\mathrm{v} - \ddot{x}_\mathrm{d}) + D_\mathrm{a}(\dot{x}_\mathrm{v} - \dot{x}_\mathrm{d}) + K_\mathrm{a}(x_\mathrm{v} - x_\mathrm{d}) = F_\mathrm{p}, \quad (1)$$

where M_a, D_a, and K_a are the virtual mass, viscous damping constant and spring constant, respectively; $x_\mathrm{v}, \dot{x}_\mathrm{v}$, and $\ddot{x}_\mathrm{v}$ represent the position, velocity, and acceleration of the virtual object, respectively; and $x_\mathrm{d}, \dot{x}_\mathrm{d}$, and $\ddot{x}_\mathrm{d}$ denote the task-dependent reference position and its time derivatives, which are given. In this work, M_a, D_a, and K_a are set to achieve critical damping of the system, as in [13]. The virtual force F_p is defined on the basis of the proximity sensor output as follows:

$$F_\mathrm{p} = D_\mathrm{p}\frac{\dot{\xi}}{\xi}, \quad (2)$$

where ξ is the sensor output (the voltage value output for the light intensity detected by the sensor) and D_p is the virtual force gain. In the previous method [13], the virtual object's states $x_\mathrm{v}, \dot{x}_\mathrm{v}$, and $\ddot{x}_\mathrm{v}$ are used as references for the subsequent impedance controller. Specifically, the robot's motion is governed by both the proximity sensor output through the virtual dynamics (1) and the contact force through the impedance controller.

In their analysis, Arita et al. [13] employed an optical proximity sensor output model based on the inverse square law (negative nth power model), expressed as follows:

$$\xi = \frac{\alpha\beta\psi}{(l + l_0)^n}, \quad (3)$$

where α is the reflectance of the object, β is the transform coefficient of the light intensity received by a photodiode in relation to the voltage value, ψ is the energy of the light emitted from the LED, and l is the distance between the robot's contact surface and the target object's contact surface. Setting the positive x-direction as pointing away from the sensor, $l = x_\mathrm{o} - x$, where x_o is the contact surface position of the colliding object, and x is the contact surface position of the robot. We refer to the contact part of the robot as "the plant" because it is the control target in this letter, and this part may be distinct from the main body of the robot, such as fingertips or foot endpoints. Moreover, l_0 is the offset distance between the proximity sensor and the contact surface of the plant, and n is the diffusion coefficient. This model has been used in several related works [17], [18], [19].

We focus on impact mitigation motion prior to contact, which is governed primarily by (1). When the frictional forces and modeling errors are negligible and no contact force is present, the tracking error of the impedance controller can be disregarded. Therefore, in our analyses and simulations, we assume that the actual plant motion coincides with the virtual object motion, i.e., $x = x_\mathrm{v}$.

Consequently, the impact mitigation motion model containing the challenges to be addressed in this study is represented as

IEEE Robotics and Automation Letters (RA-L) paper, presented at ICRA 2026, Vienna, Austria. Cite as RA-L paper.

follows:

$$M_{\mathrm{a}}(\ddot{x}-\ddot{x}_{\mathrm{d}})+D_{\mathrm{a}}(\dot{x}-\dot{x}_{\mathrm{d}})+K_{\mathrm{a}}(x-x_{\mathrm{d}})=-nD_{\mathrm{p}}\frac{\dot{l}}{l+l_0}. \tag{4}$$

Understanding the relationships between plant motion and parameters is important for parameter optimization through conventional approaches such as numerical optimization methods. However, owing to the discontinuous, nonautonomous, and nonlinear nature of the differential equation (4), neither analytical solutions nor direct relationship analysis is feasible. Notably, Arita et al. [13] proposed methods for designing admittance parameters (M_{a}, D_{a}, and K_{a}) on the basis of the zero-input response analysis, whereas n is determined through static sensor calibration. Therefore, this study focuses on the design of the virtual force gain D_{p}.

III. Parameter Optimization Method With Exponential Function-Based Sensor Models

In (4), the analytical challenges arise from its right-hand side, specifically from the sensor output model given by (3). Our key approach is to replace (3) with an alternative sensor output model that both adequately approximates the actual sensor characteristics and renders (4) more mathematically tractable.

A. Approximate Models of Proximity Sensor Outputs

We employ two sensor output models to reformulate (4). The first model is formulated as follows:

$$\xi=a_1\exp(c_1 l), \tag{5}$$

where $a_1>0$ and $c_1<0$ are approximate parameters and a_1 includes the reflectance in comparison with (3). We refer to (5) as the 1st-order exponential model because of its first-order polynomial exponent. Notably, (5) was previously proposed by Suzuki et al. [21] as an approximate model for reflective optical proximity sensors. Our study demonstrates that (5) improves the mathematical tractability of (4).

For the second model, we propose a novel sensor output model that achieves higher approximation accuracy than (5). While more complex models generally provide higher approximation accuracy than simple ones, excessive complexity may reduce mathematical tractability. Therefore, we employ an exponential function with a second-order polynomial exponent and refer to it as the 2nd-order exponential model. In the following sections, we demonstrate the superior approximation accuracy of the 2nd-order exponential model and its contribution to the analysis of (4). The 2nd-order exponential model is represented as follows:

$$\xi=a_2\exp(b_2 l^2+c_2 l), \tag{6}$$

where a_2, b_2, and c_2 are approximate parameters and a_2 includes the reflectance in comparison with (3).

B. Analysis Facilitated by the Exponential Function-Based Sensor Models

1) Analysis Using the 1st-Order Exponential Model: By replacing (3) with (5), we obtain the following expression instead of (4):

$$M_{\mathrm{a}}(\ddot{x}-\ddot{x}_{\mathrm{d}})+D_{\mathrm{a}}(\dot{x}-\dot{x}_{\mathrm{d}})+K_{\mathrm{a}}(x-x_{\mathrm{d}})=c_1D_{\mathrm{p}}\dot{l}. \tag{7}$$

Equation (7) can be reformulated by considering x_{d} as the reference coordinate as follows:

$$M_{\mathrm{a}}\ddot{l}+(D_{\mathrm{a}}+c_1D_{\mathrm{p}})\dot{l}+K_{\mathrm{a}}l=M_{\mathrm{a}}\ddot{\bar{x}}_{\mathrm{o}}+D_{\mathrm{a}}\dot{\bar{x}}_{\mathrm{o}}+K_{\mathrm{a}}\bar{x}_{\mathrm{o}}, \tag{8}$$

where $\bar{x}_{\mathrm{o}}=x_{\mathrm{o}}-x_{\mathrm{d}}$, $l=x_{\mathrm{o}}-x=\bar{x}_{\mathrm{o}}-\bar{x}$, and $\bar{x}=x-x_{\mathrm{d}}$.

In this analysis, we assume

$$\bar{x}_{\mathrm{o}}=\frac{1}{2}\bar{a}_{\mathrm{o}}t^2+\bar{v}_{\mathrm{o,i}}t+\bar{x}_{\mathrm{o,i}}. \tag{9}$$

where t is the time elapsed since the moment when the colliding object enters the detection range of the proximity sensor, $\bar{a}_{\mathrm{o}}$ is the acceleration of the object with respect to the reference coordinate x_{d}, $\bar{v}_{\mathrm{o,i}}$ is its initial velocity, and $\bar{x}_{\mathrm{o,i}}$ is its initial position when it enters the detection range, with respect to x_{d}. This assumption renders (8) a linear differential equation that can be exactly solved and with broad applicability. For example, the applicable scenarios include impact mitigation when a proximity sensor is attached to the foot of a freely falling robot [11], and impact reduction when a robot catches an object thrown to it. Moreover, setting $\bar{a}_{\mathrm{o}}=0$ represents scenarios in which a plant approaches the contact object at a desired velocity, and further setting $\bar{v}_{\mathrm{o,i}}=0$ includes scenarios in which a fixed object is present when the plant approaches the target position. The latter scenarios are similar to the grasping control case described in [14].

On the basis of the above assumption, the exact solution of (8) is as follows:

$$l=\frac{\lambda_2X_1-X_2}{\lambda_2-\lambda_1}\exp(\lambda_1 t)+\frac{X_2-\lambda_1X_1}{\lambda_2-\lambda_1}\exp(\lambda_2 t)-\frac{c_1D_{\mathrm{p}}}{K_{\mathrm{a}}}\left\{\bar{a}_{\mathrm{o}}t+\bar{v}_{\mathrm{o,i}}-\frac{\bar{a}_{\mathrm{o}}}{K_{\mathrm{a}}}(D_{\mathrm{a}}+c_1D_{\mathrm{p}})\right\}+\bar{x}_{\mathrm{o}}, \tag{10}$$

$$X_1=\epsilon-\bar{x}_{\mathrm{o,i}}+\frac{c_1D_{\mathrm{p}}}{K_{\mathrm{a}}}\left\{\bar{v}_{\mathrm{o,i}}-\frac{\bar{a}_{\mathrm{o}}}{K_{\mathrm{a}}}(D_{\mathrm{a}}+c_1D_{\mathrm{p}})\right\}, \tag{11}$$

$$X_2=\mu-\bar{v}_{\mathrm{o,i}}+\frac{c_1D_{\mathrm{p}}}{K_{\mathrm{a}}}\bar{a}_{\mathrm{o}}, \tag{12}$$

$$\lambda_{1,2}=\frac{-(D_{\mathrm{a}}+c_1D_{\mathrm{p}})\pm\sqrt{(D_{\mathrm{a}}+c_1D_{\mathrm{p}})^2-4M_{\mathrm{a}}K_{\mathrm{a}}}}{2M_{\mathrm{a}}}, \tag{13}$$

where ϵ and μ are the initial values of l and $\dot{l}$, respectively.

2) Analysis Using the 2nd-Order Exponential Model: By replacing (3) with (6), we obtain the following expression instead of (4):

$$M_{\mathrm{a}}(\ddot{x}-\ddot{x}_{\mathrm{d}})+D_{\mathrm{a}}(\dot{x}-\dot{x}_{\mathrm{d}})+K_{\mathrm{a}}(x-x_{\mathrm{d}})=D_{\mathrm{p}}(2b_2l+c_2)\dot{l}. \tag{14}$$

Although (14) is a nonlinear differential equation, it becomes tractable by assuming the obstacle motion has a constant velocity with respect to the coordinate x_{d}. On the basis of this assumption, (14) is reformulated as follows:

$$M_{\mathrm{a}}\ddot{l}+D_{\mathrm{a}}\dot{l}+K_{\mathrm{a}}l+2b_2D_{\mathrm{p}}\dot{l}l+c_2D_{\mathrm{p}}\dot{l}=K_{\mathrm{a}}\bar{v}_{\mathrm{o}}t+D_{\mathrm{a}}\bar{v}_{\mathrm{o}}+K_{\mathrm{a}}\bar{x}_{\mathrm{o,i}}, \tag{15}$$

where $\bar{v}_{\mathrm{o}}$ is the constant obstacle velocity. On the basis of the results of preliminary experiments, we find that uniform motion can be a solution to (15). Let the candidate solution be expressed as follows:

$$l=At+B, \tag{16}$$

IEEE Robotics and Automation Letters (RA-L) paper, presented at ICRA 2026, Vienna, Austria. Cite as RA-L paper.

where A and B are constant values. The result of substituting (16) into (15) is regarded as an identical equation for t, and the following equation is obtained by solving the identical equation:

$$A = \frac{-K_\mathrm{a} \pm \sqrt{8b_2 D_\mathrm{p} \bar{v}_\mathrm{o} K_\mathrm{a} + K_\mathrm{a}^2}}{4b_2 D_p}, \tag{17}$$

$$B = \frac{D_\mathrm{a}\bar{v}_\mathrm{o} + K_\mathrm{a}\bar{x}_{o,i} - c_2 D_\mathrm{p} A - D_\mathrm{a} A}{2b_2 D_\mathrm{p} A + K_\mathrm{a}}. \tag{18}$$

Since there are two possible solutions for A, we determine the appropriate sign of (17) that satisfies $0 \leq |A| \leq |\bar{v}_\mathrm{o}|$ on the basis of the contact condition between the plant and the obstacle. Furthermore, on the basis of the definition of l, our assumption (i.e., $\bar{x}_\mathrm{o} = \bar{v}_\mathrm{o} t + \bar{x}_{\mathrm{o,i}}$), (16), (17), and (18), the relationship between the plant position $\bar{x}$ and relative distance l can be expressed as follows:

$$\bar{x} = \frac{\bar{v}_\mathrm{o} - A}{A} l + \frac{c_2 D_p \bar{v}_o A - D_\mathrm{a}\bar{v}_\mathrm{o}^2 + D_\mathrm{a}\bar{v}_\mathrm{o} A}{(2b_2 D_\mathrm{p} A + K_\mathrm{a})A}. \tag{19}$$

C. Optimization for Parameter Design

We use the obtained solutions to the differential equation describing the impact mitigation motion to determine the optimal gain D_p on the basis of performance trade-offs. To maximize the mitigation performance, D_p should be designed to minimize $\dot{l}$ when $l = 0$. However, there is a cost associated with considering impact mitigation motion. For example, in the case of an approaching obstacle, impact mitigation requires a certain range of motion, whereas in the case of a plant approaching an obstacle, impact mitigation requires additional time so that contact occurs at a reduced speed.

For the former case, we represent the optimization problem as follows:

$$\underset{D_\mathrm{p}}{\text{minimize}} \quad f_1(D_\mathrm{p}) := w_1 \left(\frac{x}{x_\mathrm{typ}}\right)^2 + w_2 \left(\frac{\dot{l}}{\dot{l}_\mathrm{typ}}\right)^2, \tag{20}$$

$$\text{subject to} \quad l = 0, \tag{21}$$

where w_1 and w_2 are weights and x_typ and $\dot{l}_\mathrm{typ}$ are the typical values for normalization. We can determine these typical values on the basis of the maximum range of motion or the expected obstacle velocity. Notably, determining these values with high accuracy is unnecessary. The normalization process facilitates the setting of weights without considering scale adjustments.

Similarly, for the latter case, we formulate the optimization problem as follows:

$$\underset{D_\mathrm{p}}{\text{minimize}} \quad f_2(D_\mathrm{p}) := w_3 \left(\frac{t}{t_\mathrm{typ}}\right)^2 + w_4 \left(\frac{\dot{l}}{\dot{l}_\mathrm{typ}}\right)^2, \tag{22}$$

$$\text{subject to} \quad l = 0, \tag{23}$$

where w_3 and w_4 are weights and t_typ is the typical value used for normalization. For example, we can set t_typ on the basis of the desired task time.

IV. Evaluation of the Models

A. Objective of Model Evaluation

In the previous section, the contributions of the 1st-order and 2nd-order exponential models to analytics were explored. The 1st-order exponential model is applicable to broader situations than the 2nd-order model is. However, whether this advantage is helpful depends on a user's target application. On the other hand, although the 2nd-order exponential model can better express actual sensor outputs more accurately than the 1st-order model can, the required accuracy depends on the specific application. In this section, the accuracy of these two models is analyzed and compared to facilitate proper model selection.

First, a collision experiment is conducted to obtain sample data. Next, we use these data to evaluate the accuracy of the two models in terms of fitting the actual sensor output. Then, we assess the motion approximation accuracy of the solutions from Sections III-B1 and III-B2. In this work, we conducted a collision experiment for the dual purpose of acquiring data for parameter identification and obtaining actual data for impact mitigation motion. However, a collision experiment is unnecessary to identify the model parameters, as sufficient data can be obtained via a static experiment to measure the relationship between the sensor output and distance.

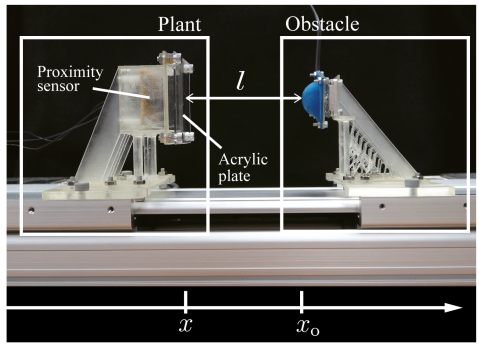

Fig. 2. Experimental setup for the evaluation of the models in Section IV. This setup is identical to that used in a previous study [13]. It is used for parameter identification and the evaluation of approximation accuracy. A separate setup is used for verification of the optimal gains.

B. Experimental Setup for Model Evaluation

The experimental device is the same as that used in [13]. Fig. 2 shows the device, which consists of dual independent linear stages (SLP-15-300-D-M3-A3-SH, Nippon Pulse Motor Co., Ltd., Tokyo, Japan) involving the plant and the obstacle. A reflected-light-intensity proximity sensor was installed on the plant. The sensor consisted of three LEDs and phototransistors (RPR-220, ROHM Co., Ltd., Kyoto, Japan) to improve the signal-to-noise ratio. Moreover, to reduce sensor noise, we used a median filter with a sliding window length of 10 and a fifth-order Butterworth low-pass filter with a cutoff frequency of 500 Hz. The sensor output characteristics change beyond the focal distance. Therefore, we recessed the sensor from the contact point and attached a transparent acrylic plate to ensure the sensor would only operate in the range beyond the focal distance. To remove the influence of the acrylic plate, the sensor output was offset so that the output was 0 V when the sensor did not detect the obstacle. The obstacle was a hemispherical object with a diameter of 20 mm. We confirmed that the obstacle shape slightly affects the sensor output because the detection angle of the proximity sensor used in the experiments is narrow. Thus, we chose an object with a hemispherical shape so that we could

IEEE Robotics and Automation Letters (RA-L) paper, presented at ICRA 2026, Vienna, Austria. Cite as RA-L paper.

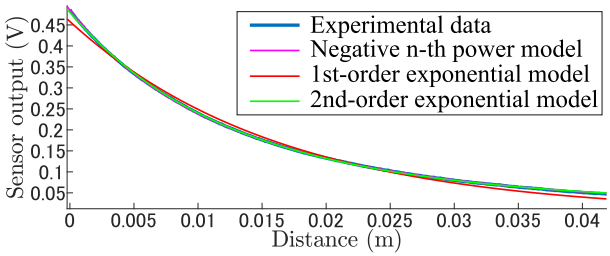

Fig. 3. Comparison of the experimental data and sensor output models as a function of distance. The blue line represents the experimental data, the magenta line represents the results of the negative *n*th power model, the red line represents the results of the 1st-order exponential model, and the green line represents the results of the 2nd-order exponential model.

TABLE I
IDENTIFIED PARAMETERS OF THE THREE PROXIMITY SENSOR OUTPUT MODELS

Model	Parameter	R-squared
Negative n-th power model	$\alpha\beta\psi$=1.30 × 10^{-5}	0.9999
	l_0=0.0419	
	n=3.32	
1st-order exponential model	a_1=0.458	0.9952
	c_1=−61.0	
2nd-order exponential model	a_2=0.480	0.9999
	b_2=474	
	c_2=−74.0	

uniquely define the contact point for evaluation. Notably, although the output characteristics and/or dependence on obstacle sizes/shapes may differ from those of different sensors, these considerations are related to sensor design, which is beyond the scope of this letter. A control computer (MicroLabBox, dSPACE GmbH, Paderborn, Germany) was used to obtain the proximity sensor data at 10 kHz. The computer also acquired encoder data and controlled position in each stage of motion via motor drivers (MADLT11SM, Panasonic Industry Company, Ltd., Osaka, Japan).

The plant and the obstacle were initially separated by 0.0422 m. The obstacle approached the plant with a uniform motion of -0.3 m/s because the solution when the 2nd-order exponential model is used assumes uniform motion of the obstacle. The plant's reference position was fixed at 0 m, and the initial plant position was also 0 m. The plant was controlled using the impact mitigation method [13]. In summary, the initial conditions for (10) and (19) are $x_\mathrm{d} = 0$ m, $\dot{x}_\mathrm{d} = 0$ m, $\ddot{x}_\mathrm{d} = 0$ m/s^2, $\bar{a}_\mathrm{o} = 0$ m/s^2, $\bar{v}_\mathrm{o,i} = \bar{v}_\mathrm{o} = \mu = -0.3$ m/s, and $\bar{x}_\mathrm{o,i} = \epsilon = 0.0422$ m. Moreover, the parameters in (1) were $M_\mathrm{a} = 1$ kg, $D_\mathrm{a} = 10$ N·s/m, $K_\mathrm{a} = 25$ N/m, and $D_\mathrm{p} = -1.0$ N·s. We set the parameters to ensure that the device would not be damaged. Although we collected data three times, the repetition accuracy of the data was satisfactory; therefore, we present only one representative dataset for ease of interpretation.

C. Comparison of the Sensor Output Models

We compared the three proximity sensor models shown in (3), (5), and (6). Fig. 3 and Table I show the comparison of the results. We evaluated the accuracy of the models based on the coefficient of determination (R-squared). The R-squared value of the negative *n*th power model and 2nd-order exponential model was 0.9999; therefore, the model results matched observation, without almost no error. The accuracy of the 1st-order exponential model was slightly lower than that of the other two models. However, the R-squared value was 0.9952. The error was still small.

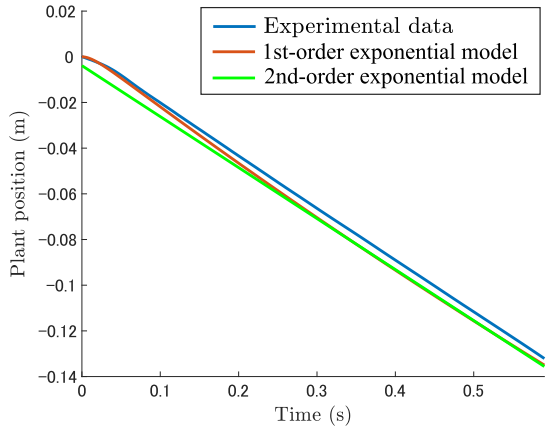

Fig. 4. Time dependence of the plant position from the start of obstacle operation to collision. The blue line represents the experimental data, the red line represents the result obtained with the 1st-order exponential model, and the green line represents the result obtained with the 2nd-order exponential model.

D. Comparison of the Motion Solutions in Terms of Accuracy

Fig. 4 shows the result of comparing the model of the plant position using the 1st- and 2nd-order exponential models with the experimental data from the start of the obstacle approach motion. The model was solved by substituting the parameters noted in Section IV-B and the approximate parameters of the sensor output obtained in Section IV-C into (10) or (19), and l was converted into the plant position x. The R-squared value of the 1st-order exponential model was 0.992, and that of 2nd-order exponential model was 0.984. Thus, the error was small in both cases. In practice, the value during collisions is important for designing the parameters. On the basis of the plant position at the collision site shown on the right side of Fig. 4, the experimental result was determined to be -0.132 m, the analysis result using the 1st-order exponential model was determined to be -0.135 m with an error of 3 mm, and the analysis result using the 2nd-order exponential model was determined to be -0.136 m with an error of 4 mm.

Fig. 5 shows the comparison of the relative velocity $\dot{l}$. We evaluate the impact mitigation effect on the basis of the ratio $\dot{l}/v_\mathrm{o}$, which compares the relative velocity when impact mitigation control is used with that when control is not used. On the basis of the values on the far right side of Fig. 5, the ratio is 78.0 % for the experimental result, 70.4 % for results of the the 1st-order model, and 74.4 % for the results of the 2nd-order model. With the experimental value as the true value, the relative errors are 9.74 % for the 1st-order model and 4.62 % for the 2nd-order model.

V. EVALUATION OF THE OPTIMIZATION

We verified that the optimal virtual force gain D_p can be obtained using the approximate models: the 1st- and/or 2nd-order exponential models. When the 1st-order exponential model is used, the constraint ($l = 0$) is treated as a nonlinear equality constraint. On the other hand, when the 2nd-order model is used, we can directly substitute $l = 0$ into the solution (19). A common

IEEE Robotics and Automation Letters (RA-L) paper, presented at ICRA 2026, Vienna, Austria. Cite as RA-L paper.

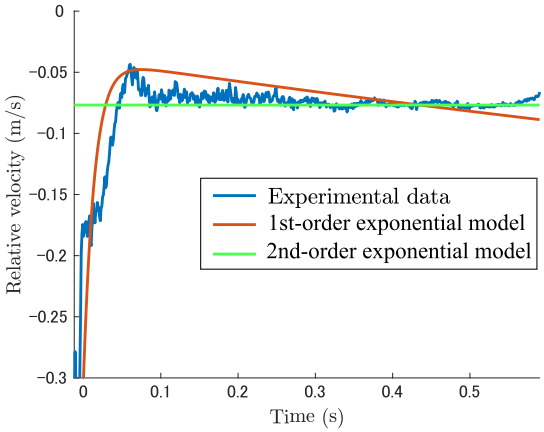

Fig. 5. Time dependence of the relative velocity between the plant and the obstacle from the start of the obstacle approach motion. The blue line represents the experimental data, the red line represents the results obtained with the 1st-order exponential model, and the green line represents the results obtained with the 2nd-order exponential model.

TABLE II
VIRTUAL FORCE GAIN COMPARISON FOR THE CASE OF AN APPROACHING OBSTACLE

D_p	-0.1	-0.6	-0.7	-0.8	-0.9	-10
$x\|_{t=0}$	-0.011	-0.080	-0.082	-0.103	-0.114	-0.611
$\dot{l}\|_{t=0}$	-0.199	-0.088	-0.082	-0.077	-0.072	-0.023
$f_1(D_\mathrm{p})$	0.442	0.111	0.107	0.107	0.110	1.49

optimization solver, such as MATLAB's *fmincon*, can be used for both cases.

In this letter, we explored two scenarios to verify optimality. The first scenario is the same as the experiment shown in Section IV-B, except for the D_p setting: the obstacle is approaching the stopping plant and the plant moves backward to mitigate the impact. This scenario is similar to that evaluated in [13]. Since a larger magnitude of virtual force gain tends to result in more extensive backward motion, we employ simulations for this scenario to be able to compare the optimal virtual force gain with larger magnitude gains that would be infeasible in our physical experimental setup owing to range of motion limitations. In these simulations, we employed the negative *n*th power model (4) as the sensor model. On the other hand, the second scenario was verified via an actual experiment. This scenario was similar to the grasping scenario in [14]: the plant is initially far from the desired position x_d and the obstacle disrupts the plant's motion. In the second scenario, since a larger magnitude of virtual force gain merely reduces the velocity of motion, the experimental setup does not restrict conditions. However, only the 1st-order exponential model is applicable in this scenario.

A. Results for the Approaching Obstacle Scenario

We employ (20) as the objective function, setting the parameters $w_1 = 1, w_2 = 1, x_\mathrm{typ} = -0.5$, and $\dot{l}_\mathrm{typ} = -0.3$ with reference to the experimental conditions in [13]. The optimal virtual force gain is -0.8 N·s when the 1st-order exponential model is used and -0.7 N·s when the 2nd-order exponential model is used. Table II shows a comparison of the results with several gains. These results indicate that increasing the gain reduces the relative speed but increases plant movement, whereas decreasing the gain has the opposite effect, causing premature contact before sufficient speed reduction. The objective function approaches its minimum value at a gain of -0.7 N·s or -0.8 N·s, confirming the optimality of the gains identified through our proposed models.

Furthermore, practical insights were obtained through the optimization process: we can achieve near-optimal gains without prior knowledge of the obstacle's velocity. Fig. 6 shows the optimal virtual force gains obtained when the obstacle velocity is varied from -0.01 to -1.00 m/s in increments of -0.01 m/s. The optimal gain minimally changed when the obstacle speed was faster than 0.2 m/s and remained almost the same when either the 1st- or 2nd-order exponential model was used.

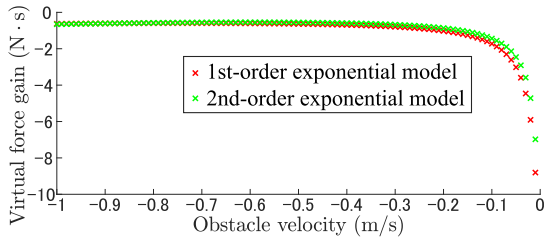

Fig. 6. Variation in optimal virtual force gains (D_p) with varying velocity. Red markers represent optimal gains obtained using the 1st-order exponential model, and green markers represent optimal gains obtained using the 2nd-order exponential model.

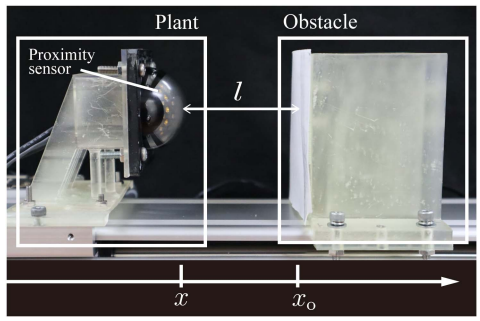

Fig. 7. Experimental setup for evaluating optimality. The obstacle is fixed and has a force sensor embedded in the surface that contacts the plant. The plant has a hemispherical fingertip shape and incorporates a proximity sensor. These are the same devices used in [14].

B. Experimental Setup for the Tracking Motion Disruption Scenario

Fig. 7 shows the experimental setup for the tracking motion disruption scenario. The devices are the same as those described in Section IV-B, except for the proximity sensor and the obstacle. Although the proximity sensor is designed for a robot finger, its features are the same as those described in Section IV-B in this letter. The fitting parameters are $a_1 = 1.25, c_1 = -63.46$. The obstacle is fixed at $x_\mathrm{o,i} = -0.035$. A force sensor (USL06-H5-200N-C, Tec Gi Han Co., Ltd., Ibaraki, Japan) is attached to the surface of the obstacle. From this experimental setup, the parameters of (10) are $x_\mathrm{d} = 0\,\mathrm{m}, \dot{x}_\mathrm{d} = \bar{v}_\mathrm{o,i} = \mu = 0\,\mathrm{m/s}, \ddot{x}_\mathrm{d} = \bar{a}_\mathrm{o} = 0\,\mathrm{m/s^2}, \bar{x}_\mathrm{o,i} = -0.035\,\mathrm{m}$, and $\epsilon = 0.065\,\mathrm{m}$. Moreover, the parameters of (1) are the same as those in Section V-A. All the settings are with reference to the experimental conditions in [14].

IEEE Robotics and Automation Letters (RA-L) paper, presented at ICRA 2026, Vienna, Austria. Cite as RA-L paper.

TABLE III
COMPARISON OF VIRTUAL FORCE GAINS FOR TRACKING MOTION DISRUPTION

D_p	-0.1	-0.5	-0.6	-0.7	-1.0	-10
t_c	0.94	2.24	2.61	2.76	3.52	38.9
F_im	3.65	1.82	1.00	0.89	0.80	-

C. Results for the Tracking Motion Disruption Scenario

We employ (22) as the objective function, with parameters $w_3 = 1$, $w_4 = 1$, $t_\mathrm{typ} = 1$, and $\dot{l}_\mathrm{typ} = -0.01$. The optimal virtual force gain is $-0.6\,\mathrm{N{\cdot}s}$. Table III compares the results obtained with similar gain values, using the average of three trials for evaluation. In Table III, we compare the contact initiation t_c and the impact force F_im instead of $t|_{l=0}$, $\dot{l}|_{l=0}$ because it is difficult to determine when $l = 0$ in the actual experiment. In this work, we define the contact initiation t_c as the instant when the force sensor output exceeds the noise level, and the impact force F_im as the peak value of the force sensor output. Notably, we are often unable to identify the peak value due to successful impact mitigation, as seen in the experimental results of [14]. If the peak value is absent, we denote the result with a hyphen in Table III.

Since we cannot directly compare $f_2(D_\mathrm{p})$, we assessed the effectiveness of changing the gain value. As shown in Table III, changing the gain value from -0.5 to -0.6 reduces the impact force by 45 % and increases the contact initiation by 17 %, whereas changing it from -0.6 to -0.7 increases the contact initiation by 6 % while reducing the impact force by only 11 %. If we define the impact-time trade-off factor as the reduced force ratio divided by the increased time ratio, the values are 2.65 for the former case and 1.83 for the latter case. Therefore, we can confirm that setting the gain value to the optimal gain of -0.6 effectively reduces the impact force while minimizing motion delay.

VI. DISCUSSION

A. Comparison of the Two Exponential-Based Models

In terms of the approximation accuracy of the proximity sensor output, Section IV-C demonstrates that the 2nd-order exponential model is superior to the 1st-order model. However, the results in Section IV-C demonstrate that the accuracy of the 1st-order exponential model is sufficiently high, and in Section IV-D and Section V-A, especially in Fig. 6, it is verified that the accuracy difference only slightly affects the simulation of impact mitigation motion and the determination of the optimal virtual force gain.

While the 2nd-order exponential model is superior for sensor output modeling, the 1st-order model yields solutions under a wider range of conditions, as demonstrated in Section III-B1. The assumption required to determine the solution is that the obstacle motion relative to the reference coordinate x_d can be represented as motion with uniform acceleration. This assumption can be applied to landing after free fall, catching a thrown ball, approaching an object at a constant velocity, and grasping, as shown in [14].

The analysis of more complex motion should be addressed in future work. However, this letter's method can be applied as long as the motion just before collision is covered by our assumption. For example, we can apply the method in a multicontact scenario (repetitive instances of contact with short durations) by considering the approaching phase after the separation phase.

A noteworthy aspect of the solution determined using the 2nd-order exponential model should be addressed. Although the differential equation reformulated with the 2nd-order exponential model (15) is superior to the conventional model (4) in terms of tractability because (15) is continuous, it is still nonlinear. In general, solutions of nonlinear differential equations may exhibit extreme sensitivity to initial conditions, where infinitesimal differences can lead to vastly divergent trajectories over time. In response, we confirmed through numerical simulation that the solutions expressed by (16), (17), and (18) are associated with the attraction of surrounding orbits.

B. Optimization With Additional Conditions

We can further consider limitations, such as the robot's range of motion and maximum relative velocity, as inequality constraints in the optimization process. These constraints can be directly input into the MATLAB *fmincon* solver used in this research.

Moreover, in this letter, we used the relative velocity as the index of impact mitigation because the physical properties of the obstacle are necessary to directly calculate the impact force but are usually unknown. However, we can use the impact force in the optimization process if these physical properties are known. This replacement of the relative velocity with the impact force allows us to consider the desired impact force as $F_\mathrm{im,typ}$ in the objective function and its limitations, such as the maximum impact force, as inequality constraints.

C. Determination of the Optimal Gain Despite Uncertainty in the Obstacle Velocity

Fig. 6 suggests that when an obstacle moves quickly, the gain requires minimal adjustment. Although when the obstacle moves slowly, a gain with a larger absolute value is needed compared to when the object speed is fast, even if we applied a small absolute gain for a slow obstacle, a significant impact mitigation force would not occur because the obstacle motion state is inherently safe. Therefore, we can design the gain on the basis of the optimization results for fast obstacles. Specifically, we can design the gain even when the obstacle behavior is not precisely known in advance.

VII. CONCLUSION

We established an optimal parameter design method to maximize impact mitigation performance without requiring preliminary collision trials. We demonstrated that a common optimization solver can be used because of the increased mathematical tractability achieved by representing the proximity sensor output model with two exponential function-based models: one with first-order exponents and another with second-order exponents. We verified the optimality of this approach through evaluations in two scenarios: an approaching obstacle scenario using simulations and a tracking motion disruption scenario through actual experiments.

In this research, we considered a 1-D model. This is a basic approach that can be applied to various robots. We envision using the knowledge obtained from this research for applications involving robot hands, legged robots, and collaborative robots that can achieve both fast movement and impact mitigation. For

example, it may be possible to apply the proposed strategy to legged robots on the basis of [11].

Additionally, for applications to a multi-DoF robot, it is necessary to consider the robot's motion subspace; for this purpose, we anticipate that the proposed method can be extended on the basis of previous research on force control [23]. Notably, it is desirable to consider the effect of inertia since it is related to the impact force and is affected by the robot's posture. However, even in that case, the relative velocity should be prioritized over inertia because the minimum inertia is bounded by the properties of the robot's body, whereas the relative velocity can theoretically be reduced to almost zero.

When a proximity sensor based on reflected light intensity is used, a conversion method that can reduce the influence of reflectance is important. The models used in this research allow us to express the corresponding formula in a simple form. Therefore, we believe that these models will also be useful when employing such sensors for other control approaches. Furthermore, the analysis technique applied in this study, which linearizes motion dynamics without directly linearizing the sensor model, can also be helpful for determining and designing other types of virtual forces.

REFERENCES

[1] M. Suomalainen et al., "A survey of robot manipulation in contact," *Robot. Auton. Syst.*, vol. 156, 2022, Art. no. 104224.

[2] Y. Sato, E. Ohashi, and K. Ohnishi, "Impact force reduction for hopping robot," in *Proc. 31st Annu. Conf. IEEE Ind. Electron. Soc.*, 2005, pp. 1821–1826.

[3] G. A. Cardona et al., "Reduction of impact force in falling robots using variable stiffness," in *Proc. SoutheastCon*, 2016, pp. 1–6.

[4] S. Haddadin, A. De Luca, and A. Albu-Schäffer, "Robot collisions: A survey on detection, isolation, and identification," *IEEE Trans. Robot.*, vol. 33, no. 6, pp. 1292–1312, Dec. 2017.

[5] G. Pang et al., "CoboSkin: Soft robot skin with variable stiffness for safer human–robot collaboration," *IEEE Trans. Ind. Electron.*, vol. 68, no. 4, pp. 3303–3314, Apr. 2021.

[6] E. J. Park, G. Li, and J. K. Mills, "Development of a smart robotic gripper for shape and vibration control of flexible payloads: Theory and experiments," in *Proc. IEEE Int. Conf. Robot. Automat.*, 2003, vol. 2, pp. 2418–2423.

[7] N. G. Tsagarakis, I. Sardellitti, and D. G. Caldwell, "A new variable stiffness actuator (compAct-VSA): Design and modelling," in *Proc. IEEE/RSJ Int. Conf. Intell. Robots Syst.*, 2011, pp. 378–383.

[8] N. Hogan, "Impedance control part 1-part 3," *Trans. ASME, J. Dyn. Syst. Meas. Control*, vol. 107, pp. 1–24, 1985.

[9] J. Liang, J. Wu, H. Huang, W. Xu, B. Li, and F. Xi, "Soft sensitive skin for safety control of a nursing robot using proximity and tactile sensors," *IEEE Sensors J.*, vol. 20, no. 7, pp. 3822–3830, Apr. 2020.

[10] K. Koyama, K. Murakami, T. Senoo, M. Shimojo, and M. Ishikawa, "High-speed, small-deformation catching of soft objects based on active vision and proximity sensing," *IEEE Robot. Autom. Lett.*, vol. 4, no. 2, pp. 578–585, Apr. 2019.

[11] R. Sato, H. Arita, and A. Ming, "Pre-landing control for a legged robot based on tiptoe proximity sensor feedback," *IEEE Access*, vol. 10, pp. 21619–21630, 2022.

[12] J. R. Guadarrama-Olvera, S. Kajita, and G. Cheng, "Preemptive foot compliance to lower impact during biped robot walking over unknown terrain," *IEEE Robot. Autom. Lett.*, vol. 7, no. 3, pp. 8006–8011, Jul. 2022.

[13] H. Arita, H. Nakamura, T. Fujiki, and K. Tahara, "Smoothly connected preemptive impact reduction and contact impedance control," *IEEE Trans. Robot.*, vol. 39, no. 5, pp. 3536–3548, Oct. 2023.

[14] S. Tokiwa, H. Arita, Y. Suzuki, and K. Tahara, "Integrated grasping controller leveraging optical proximity sensors for simultaneous contact, impact reduction, and force control," *IEEE Robot. Autom. Lett.*, vol. 9, no. 12, pp. 11633–11640, Dec. 2024.

[15] H. Alagi et al., "Evaluation of on-robot capacitive proximity sensors with collision experiments for human-robot collaboration," in *Proc. IEEE/RSJ Int. Conf. Intell. Robots Syst.*, 2022, pp. 6716–6723.

[16] I. D. Walker, "Impact configurations and measures for kinematically redundant and multiple armed robot systems," *IEEE Trans. Robot. Autom.*, vol. 10, no. 5, pp. 670–683, Oct. 1994.

[17] N. Yamaguchi, S. Hasegawa, K. Okada, and M. Inaba, "A gripper for object search and grasp through proximity sensing," in *Proc. IEEE/RSJ Int. Conf. Intell. Robots Syst.*, 2018, pp. 1–9.

[18] K. Koyama, Y. Suzuki, A. Ming, and M. Shimojo, "Grasping control based on time-to-contact method for a robot hand equipped with proximity sensors on fingertips," in *Proc. IEEE/RSJ Int. Conf. Intell. Robots Syst.*, 2015, pp. 504–510.

[19] K. Koyama, Y. Suzuki, A. Ming, and M. Shimojo, "Integrated control of a multiple-degree-of-freedom hand and arm using a reactive architecture based on high-speed proximity sensing," *Int. J. Robot. Res.*, vol. 38, no. 14, pp. 1717–1750, 2019.

[20] K. Oprzdkiewicz and M. Garbacz, "Modeling of IR proximity sensors with the use of interval mittag-leffler function," *J. Automat., Mobile Robot. Intell. Syst.*, vol. 11, pp. 3–6, 2017.

[21] Y. Suzuki, R. Yoshida, T. Tsuji, T. Nishimura, and T. Watanabe, "Grasping strategy for unknown objects based on real-time grasp-stability evaluation using proximity sensing," *IEEE Robot. Autom. Lett.*, vol. 7, no. 4, pp. 8643–8650, Oct. 2022.

[22] H. Hasegawa, Y. Mizoguchi, K. Tadakuma, A. Ming, M. Ishikawa, and M. Shimojo, "Development of intelligent robot hand using proximity, contact and slip sensing," in *Proc. IEEE Int. Conf. Robot. Automat.*, 2010, pp. 777–784.

[23] M. Iskandar, C. Ott, A. Albu-Schäffer, B. Siciliano, and A. Dietrich, "Hybrid force-impedance control for fast end-effector motions," *IEEE Robot. Autom. Lett.*, vol. 8, no. 7, pp. 3931–3938, Jul. 2023.